Stability and Operation of Injection-Locked Regenerative Frequency Dividers

Mohammad Farazian, *Member, IEEE*, Prasad S. Gudem, *Member, IEEE*, and Lawrence E. Larson, *Fellow, IEEE*

***Abstract*—Injection-locked regenerative frequency dividers can achieve a fractional division ratio similar to regenerative frequency dividers and can provide quadrature output phases. An analysis of the steady-state operation, stability, and phase noise of injection-locked regenerative frequency dividers is presented. In addition, two-stage ring oscillators (based on negative-resistance delay cells) are studied, and their steady-state free-running operation and injection-locked behavior are investigated. Simulation results based on the equations derived in this paper are compared with circuit simulations to examine the accuracy of our analysis, which is quantified in different parts of this paper.**

***Index Terms*—Fractional frequency divider, inductorless design methodology, injection-locked frequency divider (ILFD), injection-locking, locking range, polyphase filter, regenerative frequency divider, ring oscillator, self-resonance frequency (SRF), single-sideband (SSB) mixer .**

I. Introduction

FREQUENCY DIVIDERS are one of the most important components of any frequency synthesizer. In some applications, fractional division ratios are required [1]–[3]. In addition, 50% duty-cycle quadrature output phases will allow the use of single-sideband (SSB) frequency conversion. It is challenging to implement a high-frequency fractional 50% duty-cycle and quadrature output frequency divider in a digital CMOS technology with small die area and low power consumption.

We begin this paper with a general overview of fractional-frequency-divider architectures in Section II. Injection-locked regenerative frequency dividers are introduced in Section III. Their stability is analyzed in Section IV. Two-stage ring oscillators are good candidates for quadrature output injection-locked regenerative frequency dividers. Their steady-state operation, stability, and injection-locked behavior (based on negative-resistance delay cells) are studied in Section V. A phase-noise analysis of the injection-locked regenerative frequency dividers is performed in Section VI. Section VII contains a design example of injection-locked regenerative dividers to implement a divider with fractional division ratio and quadrature output phases. Section VIII summarizes and concludes this paper.

II. Fractional Frequency Dividers

Fractional frequency dividers are often implemented with multimodulus frequency dividers and are used in fractional- N frequency synthesizers to implement a fractional division ratio [4]. In this technique, interpolating between two or more integer division ratios provides a division ratio that, on average, represents a fractional number [4]. Unfortunately, the output waveform achieved with this technique does not exhibit a 50% duty cycle when interpolating between different moduli of the frequency divider. Consequently, this output waveform can be used in applications such as fractional- N phase-locked loops, where the instantaneous period and the duty cycle of the signal are less important and the loop filter averages the output of the phase detector (or charge pump). However, this waveform cannot be easily used for frequency translation in mixers or in any application that is sensitive to the instantaneous period (or frequency) of the input signal. Hence, there is a need to develop frequency dividers that can *directly* generate fractional division ratios.

Regenerative frequency dividers are another technique to achieve fractional division ratios [5]. Fig. 1(a) shows a block diagram of a regenerative frequency divider. The stability and operation of regenerative frequency dividers are studied in [5]–[8]. As shown in Fig. 1(a), a mixer, or a nonlinear network in general, is used to create the mixing products of the input and output frequencies. The tuned network in the forward path passes the desired mixing product to the output. As shown in [5], this divider can achieve the desired fractional division ratio. However, regenerative frequency dividers have several limitations: 1) They are usually not able to provide quadrature output phases; 2) the sensitivity and output amplitude are degraded when higher order mixing products are needed to achieve larger than two, or fractional, division ratios [9]; 3) they often require inductively tuned loads, which require a large die area; and 4) the locking range is limited by the Q of the tuned load.

The block diagram of a frequency divider based on the heterodyne phase-locking technique [10] is shown in Fig. 1(b). This technique can also be used to obtain a fractional division ratio. However, it requires tuned loads for filtering the sum component at the output of the mixer. In addition, the divider in Fig. 1(b) requires more than one mixer to implement a fractional division ratio. Increasing the number of mixers will increase the power consumption and die area. At the same time, this frequency divider cannot provide quadrature phases of the output, unless a quadrature VCO, or a combination of a VCO at twice the desired frequency and a divide-by-two, is used in the forward path. These approaches require more area and power consumption. In addition, a quadrature VCO poses its own limitations on the I/Q amplitude and phase accuracy, as well as the achievable phase noise.

Another approach to implement a fractional division ratio is to use multiple phases of the input clock and interpolate between them using a sequential logic circuit [11]. However, the speed of this technique is limited to lower frequencies, since it relies on digital sequential circuits. Moreover, it can neither provide quadrature output phases nor achieve a 50% duty cycle.

Manuscript received May 11, 2009; revised January 11, 2010; accepted January 11, 2010. Date of publication March 22, 2010; date of current version August 11, 2010. This work was supported by the Center for Wireless Communications, University of California San Diego and its member companies. This paper was recommended by Associate Editor E. A. M. Klumperink.

M. Farazian and P. S. Gudem are with Qualcomm Inc., San Diego, CA 92121 USA (e-mail: mfarazian@gmail.com; pgudem@qualcomm.com).

L. E. Larson is with the Department of Electrical and Computer Engineering, University of California San Diego, La Jolla, CA 92093 USA (e-mail: larson@ece.ucsd.edu).

Digital Object Identifier 10.1109/TCSI.2010.2043012

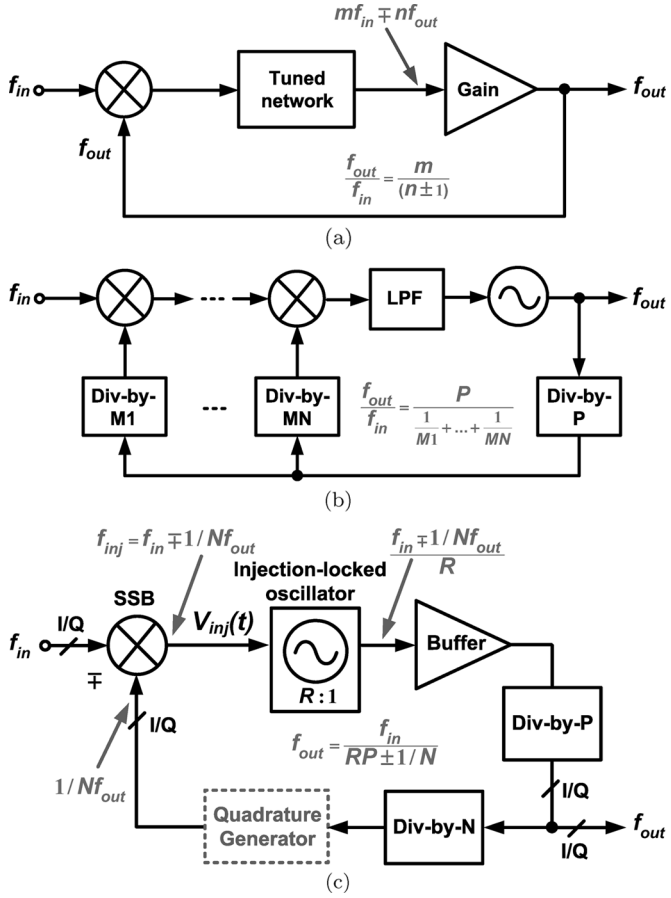

Fig. 1. (a) Block diagram of a traditional regenerative frequency divider, (b) general block diagram of a frequency divider based on heterodyne phase-locking technique [10], and (c) generalized injection-locked regenerative frequency divider.

In this paper, a different category of frequency dividers is analyzed, which can achieve both fractional division ratio and 50% duty-cycle quadrature output phases. This class of frequency dividers is discussed in Section III, and its operation and stability conditions are analyzed in Section IV.

III. Injection-Locked Regenerative Frequency Dividers

A general block diagram of the injection-locked regenerative frequency divider is shown in Fig. 1(c). This divider consists of an injection-locked oscillator in the forward path, which is followed by a frequency divider with division ratio P, and a frequency divider with division ratio N in the feedback path. The mixer in this divider functions as a frequency converter, and the signal at the output of the mixer has a component at $f_{\rm in} \mp 1/N\ f_{\rm out}$. The mixer output $V_{\rm inj}$ can injection-lock the oscillator if its amplitude is sufficiently large and its frequency $f_{\rm inj}$ is within the locking range of the oscillator.

An SSB mixer can be used in this architecture to set the mixer output to $f_{\rm in} - f_{\rm out}/N$ or $f_{\rm in} + f_{\rm out}/N$ if the quadrature phases of both signals are available. This helps eliminate the inductor-tuned load of the mixer, which eases the implementation of the frequency divider in a digital CMOS technology and expands the frequency-divider input range.

If the oscillator is injection-locked to the Rth harmonic of its output frequency, i.e., $f_{\rm inj} = Rf_{\rm out}$, the output frequency of the injection-locked regenerative frequency divider can be expressed by

$$f_{\rm out} = \frac{f_{\rm in}}{RP \pm \frac{1}{N}}. \tag{1}$$

The $\pm$ in (1) depends on whether the difference or sum of two frequencies is chosen at the SSB mixer output. Equation (1) shows the possibility of obtaining fractional division ratios using the injection-locked regenerative frequency divider in Fig. 1(c). Similarly, if the oscillator is injection-locked to its Rth subharmonic, i.e., $f_{\rm inj} = f_{\rm out}/R$, then

$$f_{\rm out} = \frac{f_{\rm in}}{\frac{P}{R} \pm \frac{1}{N}}. \tag{2}$$

As can be seen from (1) and (2), injection-locked regenerative frequency dividers can generate almost any arbitrary division ratio. Moreover, as can be observed in Fig. 1(c), it can simultaneously provide multiple division ratios. Additionally, the proper choice of the divide-by- P block, e.g., a divide-by-two, enables 50% duty-cycle quadrature outputs. An appropriate distribution of the integer part of the division ratio in (1), i.e., RP [or the R/P ratio in (2)], may provide more options that can also lead to 50% duty-cycle quadrature outputs. A design example that achieves fractional division ratios, a 50% duty cycle, and quadrature outputs is presented in Section VII.

Both (1) and (2) show the possibility of obtaining fractional division ratios. However, for the rest of this paper, our focus is on the case of superharmonic injection-locking the oscillator to its Rth harmonic, i.e., $f_{\rm inj} = Rf_{\rm out}$, since this scenario has more applications in the frequency divider arena; hence, we use (1) as the input–output frequency relationship of the frequency divider in Fig. 1.

Because of the similarities between the regenerative frequency divider in Fig. 1(a) and the injection-locked regenerative frequency divider, the divider in Fig. 1(c) is sometimes referred to as a *modified regenerative divider* [3]. However, the divider in Fig. 1(c) is a separate category of frequency divider, since it relies on an injection-locked oscillator for its operation. To clarify this point, when there is no input signal to a traditional regenerative frequency divider, it does not generate any output. In fact, as discussed in [5], this is one of the stability criteria of regenerative frequency dividers. However, in the injection-locked regenerative frequency divider in Fig. 1(c), the oscillator free-runs in the absence of an input.

IV. Stability Analysis of Injection-Locked Regenerative Frequency Dividers

To analyze the stability of the frequency divider in Fig. 1(c), we assume that the oscillator in the forward path is injection-locked to a frequency that is close to the Rth harmonic of its self-resonance frequency (SRF) and an SSB mixer is used to generate the difference (or sum) of $f_{\rm in}$ and $1/Nf_{\rm out}$. In this case, the relation between $f_{\rm out}$ and $f_{\rm in}$ is expressed by (1). In addition, we assume that the input signal is applied to the LO port of the SSB mixer. If we represent the input and output of the injection-locked regenerative frequency divider by $V_{\rm in}(t) = A_i \cos(\omega_{\rm in} t + \theta_i)$ and $V_{\rm out}(t) = A_o \cos(\omega_{\rm out} t)$, respectively, the differential mixer output $V_{\rm inj}(t)$ can be expressed as

$$V_{\rm inj}(t) = G_M Z_M A_o \cos(\omega_{\rm out} t/N) f\left[A_i \cos(\omega_{\rm in} t + \theta_i)\right] \tag{3}$$

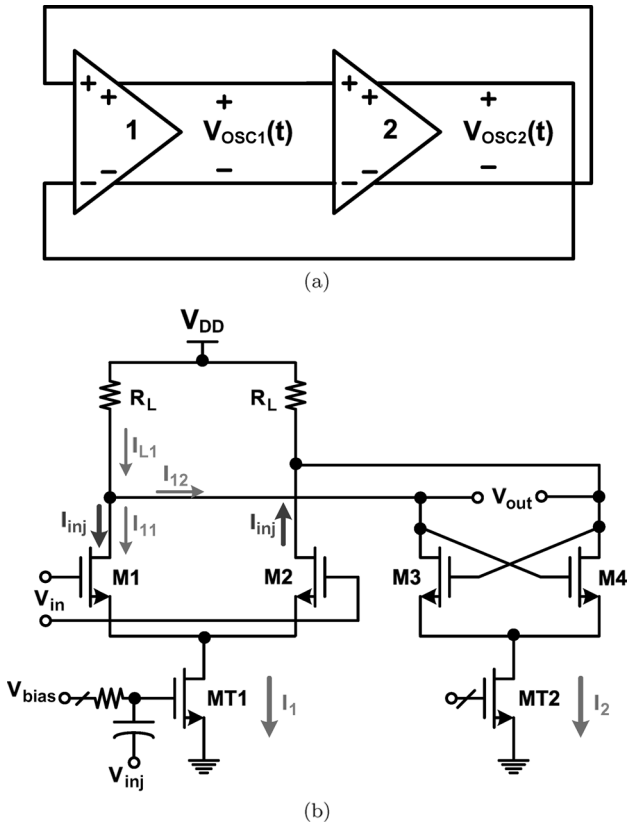

Fig. 2. Two-stage CMOS ring oscillator. (a) Block diagram. (b) Negative-resistance delay cell.

where G_M is the transconductance of the Gm stage of the SSB mixer and Z_M is the load impedance of the SSB mixer. In an inductorless design approach, Z_M is a parallel combination of the load resistor and the parasitic capacitances. Therefore, for simplicity, both Z_M and G_M can be considered constant within the locking range of the oscillator. Moreover, for simplicity, we assume that Z_M and G_M do not contribute any phase shift.

The function $f(\cdot)$ in (3) models the nonlinearity of the LO port of the mixer. If the input amplitude A_i is sufficiently large, $f(\cdot)$ can be approximated with a ± 1 square wave. Under this assumption, if we substitute the Fourier series expansion of $f[A_i \cos(\omega_{\rm in} t + \theta_i)]$ into (3), the component of $V_{\rm inj}(t)$ which is at a frequency close to the SRF of the oscillator is

$$V_{\rm inj}(t) = \frac{2}{\pi} G_M Z_M A_o \cos\left(\frac{RP}{RP \pm \frac{1}{N}} \omega_{\rm in} t + \theta_i\right). \quad (4)$$

Other mixing products at the output of the SSB mixer, which are caused by the nonlinearity of the LO port, are sufficiently far from the SRF of the oscillator; hence, they cannot injection-lock the oscillator. Linearizing the Gm stage of the mixer will suppress the mixing products caused by the nonlinearity of its transconductance (G_M). As a result, only the term shown in (4) plays a role in injection-locking the oscillator and the other terms are ignored.

Clearly, the minimum input sensitivity of the frequency divider occurs when the output frequency is $f_{\rm SRF}/P$, which corresponds to $f_{\rm in} = [RP \pm 1/N)/P] f_{\rm SRF}$, where $f_{\rm SRF}$ is the SRF of the oscillator. If the amplitude of the signal at the mixer output $(V_{\rm inj})$ is adequate to injection-lock the oscillator to $[P/(RP \pm 1/N)] f_{\rm in}$, the oscillator and the frequency divider will operate in the stable region. If the amplitude is not adequate, the oscillator is pulled and will generate sidebands [12]. As a result, the stable region of operation of the injection-locked regenerative frequency divider is determined by the locking range of the oscillator.

In order to superharmonic injection-lock an oscillator to one of the oscillator's even harmonics, the injection signal must be applied to a common-mode node [13]. For instance, in the two-stage ring oscillator in Fig. 2(a), which can be implemented using the negative-resistance delay cell in Fig. 2(b), the injection current signal must be applied to the source terminals of transistors $M1$ and $M2$. In order to do that, a common choice is to apply $V_{\rm inj}(t)$ to the gate of the tail current source of one of the delay cells in the ring oscillator. If $V_{\rm inj}(t)$ is applied to the gate of transistor $MT1$ in Fig. 2(b), the component of injection current $(I_{\rm inj}(t))$ at frequency $[P/(RP \pm 1/N)] f_{\rm in}$ that reaches the oscillator output can be found using an approach similar to [13], i.e.,

$$I_{\rm inj}(t) = \frac{8}{\pi^2 (R^2 - 1)} g_{\rm mT} G_M Z_M A_o \frac{\sin\theta_i}{\cos\chi} \times \cos\left(\frac{P}{RP \pm \frac{1}{N}} \omega_{\rm in} t - \chi\right) \quad (5)$$

where

$$\chi = \tan^{-1}(R \cot\theta_i) \quad (6)$$

and $g_{\rm mT}$ is the transconductance of $MT1$ in Fig. 2(b). The $I_{\rm inj}(t)$ expressed in (5) injection-locks the oscillator to frequency $[P/(RP \pm 1/N)] f_{\rm in}$. The magnitude of this injection current in terms of θ_i can be expressed as

$$|I_{\rm inj}(t)| = \frac{8}{\pi^2 (R^2 - 1)} g_{\rm mT} G_M Z_M A_o \sqrt{1 + (R^2 - 1)\cos^2\theta_i}. \quad (7)$$

These expressions are valid for differential oscillators where the injection signal is applied to the gate of the tail current source.

It is clear that the stable region of operation of an injection-locked regenerative frequency divider depends on the relationship between the locking range of the oscillator and the amplitude of the injection signal. This relationship is derived for LC oscillators in [12] and [14] and for ring oscillators with more than three stages in [15]–[17]. The locking range of a two-stage ring oscillator is of interest, since it requires the fewest number of delay cells to generate quadrature output phases. Consequently, it can achieve smaller die area and lower power consumption. Therefore, the free-running and injection-locked behavior of this oscillator will be studied in Section V, and its locking range for different injection-locking scenarios will be derived.

V. Injection-Locked Two-Stage Ring Oscillator

In the previous section, we showed how injection at the gate of $MT1$ generates a differential injection current at the output of the oscillator, as shown in Fig. 3. Writing the KCL at the drains of $M1$ and $M2$ of the first delay cell results in

$$\frac{V_{\rm OSC1}(t)}{R} + C \frac{\rm d}{{\rm d}t} V_{\rm OSC1}(t) = [I_{D1}(t) - I_{D2}(t)] + [I_{D3}(t) - I_{D4}(t)] + I_{\rm inj}(t). \quad (8)$$

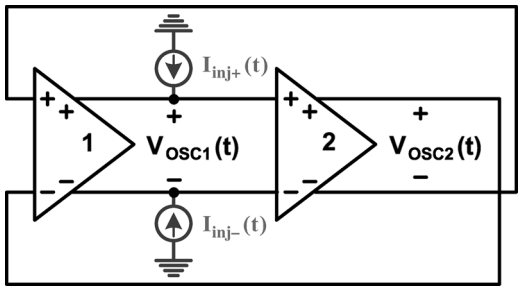

Fig. 3. Schematic of the two-stage CMOS ring oscillator when an external signal is injected at the output of the first delay cell.

In (8), $I_{\rm inj}(t)$ is the differential injection current and is defined by $I_{\rm inj_+}(t) - I_{\rm inj\_}(t)$, and R and C are the equivalent output resistance and capacitance at the output of the delay cell. A similar differential equation is obtained for the second delay cell, without the injection current, as follows:

$$\frac{V_{\rm OSC2}(t)}{R} + C\frac{\rm d}{{\rm d}t}V_{\rm OSC2}(t) = [I'_{D1}(t) - I'_{D2}(t)] + [I'_{D3}(t) - I'_{D4}(t)] \quad (9)$$

where $I'_{D1}(t)$, $I'_{D2}(t)$, $I'_{D3}(t)$, and $I'_{D4}(t)$ are the drain currents of the second delay cell.

In the steady state, $V_{\rm OSC1}(t)$ and $V_{\rm OSC2}(t)$ can be expressed using Fourier series representation, i.e.,

$$V_{\rm OSC1}(t) = \sum_{k=-\infty}^{+\infty} V1_{(2k-1)} {\rm e}^{j\theta_{1,(2k-1)}(t)} \quad (10a)$$

$$V_{\rm OSC2}(t) = \sum_{k=-\infty}^{+\infty} V2_{(2k-1)} {\rm e}^{j\theta_{2,(2k-1)}(t)} \quad (10b)$$

where

$$\theta_{1,(2k-1)}(t) = (2k-1)\omega_o t + \phi_{1,(2k-1)} \quad (11a)$$

$$\theta_{2,(2k-1)}(t) = (2k-1)\omega_o t + \phi_{2,(2k-1)}. \quad (11b)$$

In order to have a real solution for oscillator voltages, $Vi_{(2k-1)}$ and $Vi_{-(2k-1)}$ must be complex conjugates $(i = 1, 2)$.

If the values of $V_{\rm OSC1}(t)$ and $V_{\rm OSC2}(t)$ are sufficiently large, the transistors of each delay cell are fully switched and the current waveforms of $I_{D1}(t) - I_{D2}(t)$ and $I_{D3}(t) - I_{D4}(t)$ are similar to a ± 1 square wave. In this case, as shown in Appendix A, when the oscillator is injection-locked to $\omega_{\rm inj}$, i.e., $\omega_o = \omega_{\rm inj}$, the magnitude and phase of the fundamental harmonic of $V_{\rm OSC1}(t)$ can be expressed by

$$\frac{V1_1}{R} + jCV1_1\frac{{\rm d}\theta_{1,1}(t)}{{\rm d}t} = -\frac{2I_1}{\pi}{\rm e}^{j[\theta_{2,1}(t)-\theta_{1,1}(t)]} + \frac{2I_2}{\pi} + \frac{1}{2}I_{\rm inj}{\rm e}^{j[\theta_{\rm inj}(t)-\theta_{1,1}(t)]}. \quad (12)$$

A similar equation can be obtained for the second delay cell as follows:

$$\frac{V2_1}{R} + jCV2_1\frac{{\rm d}\theta_{2,1}(t)}{{\rm d}t} = \frac{2I_1}{\pi}{\rm e}^{j[\theta_{1,1}(t)-\theta_{2,1}(t)]} + \frac{2I_2}{\pi}. \quad (13)$$

To further simplify our analysis, we define $\Delta\theta$ and ψ as follows:

$$\Delta\theta \triangleq \theta_{1,1}(t) - \theta_{2,1}(t) \quad (14a)$$

$$\psi \triangleq \theta_{\rm inj}(t) - \theta_{1,1}(t). \quad (14b)$$

By separating the real and imaginary parts of (12) and (13), we obtain

$$\frac{{\rm d}\theta_{1,1}(t)}{{\rm d}t} = \frac{1}{RC}\frac{I_1\sin\Delta\theta + \frac{\pi}{4}I_{\rm inj}\sin\psi}{-I_1\cos\Delta\theta + I_2 + \frac{\pi}{4}I_{\rm inj}\cos\psi} \quad (15a)$$

$$\frac{{\rm d}\theta_{2,1}(t)}{{\rm d}t} = \frac{1}{RC}\frac{I_1\sin\Delta\theta}{I_1\cos\Delta\theta + I_2}. \quad (15b)$$

These nonlinear differential equations are very similar to those from [15] for ring oscillators with more than three stages. Equations (12) and (13) are used to calculate $V1_1$ and $V2_1$. If we represent the amplitudes of the fundamental harmonics of the first and second stages by V_{a1} and V_{a2}, i.e., $V_{a1} = 2Re[V1_1]$ and $V_{a2} = 2Re[V2_1]$; thus

$$V_{a1} = R\left(-\frac{4I_1}{\pi}\cos\Delta\theta + \frac{4I_2}{\pi} + I_{\rm inj}\cos\psi\right) \quad (16a)$$

$$V_{a2} = R\left(\frac{4I_1}{\pi}\cos\Delta\theta + \frac{4I_2}{\pi}\right). \quad (16b)$$

We use (15a) and (15b) to analyze the free-running and injection-locking behavior of the two-stage ring oscillator in Fig. 3.

A. Free-Running Oscillation

In steady state and in the absence of an external signal, i.e., $I_{\rm inj} = 0$, the ring oscillator oscillates at its SRF. In this case

$$\frac{{\rm d}\theta_{1,1}(t)}{{\rm d}t} = \frac{{\rm d}\theta_{2,1}(t)}{{\rm d}t} = \omega_{\rm SRF}. \quad (17)$$

After substituting $I_{\rm inj} = 0$ into (15a) and combining it with (15b) and (17), and from Appendix B, it is concluded that, in steady state

$$\Delta\theta = +\frac{\pi}{2}. \quad (18)$$

The SRF is obtained by substituting $\Delta\theta = +\pi/2$ into (15a) or (15b) and then

$$\omega_{\rm SRF} = \frac{1}{RC}\cdot\frac{I_1}{I_2} \quad (19)$$

and hence, the steady-state solution for $\theta_{1,1}(t)$ and $\theta_{2,1}(t)$ can be written as

$$\theta_{1,1}(t) = \omega_{\rm SRF}t \quad (20a)$$

$$\theta_{2,1}(t) = \omega_{\rm SRF}t - \frac{\pi}{2}. \quad (20b)$$

From (16a), (16b), and (18), the steady-state amplitudes of the fundamental harmonics of the output voltages are

$$V_{a1} = V_{a2} = \frac{4I_2R}{\pi}. \quad (21)$$

B. Two-Stage Ring Oscillator Under Single-Node Injection

Assuming that an external signal is injected at the output of the first delay cell of the two-stage ring oscillator, as shown

in Fig. 3, and that it has injection-locked the oscillator to its frequency ($\omega_{\rm inj}$), in this case

$$\frac{{\rm d}\theta_{1,1}(t)}{{\rm d}t} = \frac{{\rm d}\theta_{2,1}(t)}{{\rm d}t} = \omega_{\rm inj}. \tag{22}$$

We can use (22), (15a), and (15b) to find the steady-state solution for $\theta_{1,1}$ and $\theta_{2,1}$. In addition, from (15a), (15b), and (22), the oscillation frequency under injection-locking can be expressed as

$$\omega_o|_{\rm inj} = \omega_{\rm inj} = \frac{1}{RC}\frac{I_1 \sin\Delta\theta}{I_1\cos\Delta\theta + I_2}. \tag{23}$$

It is important to note that the oscillation frequency for this scenario is a function of $\Delta\theta$. Substituting the $\omega_{\rm SRF}$ from (19) into (23) results in

$$\omega_{\rm inj} = \omega_{\rm SRF}\frac{\sin\Delta\theta}{1 + RC\omega_{\rm SRF}\cos\Delta\theta}. \tag{24}$$

The corresponding phase shift ($\Delta\theta$) for any given injection frequency ($\omega_{\rm inj}$) can be found from (24). Equation (24) can be rewritten as

$$1 + \alpha\cos\Delta\theta - \beta\sin\Delta\theta = 0 \tag{25}$$

where α and β are

$$\alpha = RC\omega_{\rm SRF} \tag{26a}$$
$$\beta = \frac{\omega_{\rm SRF}}{\omega_{\rm inj}}. \tag{26b}$$

The solution for (25) can be expressed as

$$\Delta\theta = \sin^{-1}\left(\frac{1}{\sqrt{\alpha^2+\beta^2}}\right) - \tan^{-1}\left(\frac{\alpha}{\beta}\right). \tag{27}$$

Equation (27) determines the phase difference between the fundamental component of the output voltages ($V_{\rm OSC1}$ and $V_{\rm OSC2}$). As can be seen from (27), injection-locking a two-stage ring oscillator to any frequency other than its SRF (using this scheme of injection-locking) results in nonquadrature fundamental harmonics of the outputs. As an example, a two-stage ring oscillator based on the delay cell in Fig. 2(b) is designed in a 0.13-μm CMOS technology using a 1.2-V supply and is used to verify this conclusion through simulation. In this oscillator, $R_L = 500\ \Omega$, $I_1 = 1.25$ mA, $I_2 = 650\ \mu$A, and the SRF is approximately 4 GHz. The calculated output phase difference for a prototype two-stage ring oscillator is shown in Fig. 4 and compared with the circuit simulation, and the calculation error is less than 2° over the entire locking range.

We now calculate the required minimum amplitude and phase of the external signal to injection-lock the oscillator to $\omega_{\rm inj}$. From (15a), (15b), and (22), it can be concluded that

$$\frac{I_1\sin\Delta\theta + \frac{\pi}{4}I_{\rm inj}\sin\psi}{-I_1\cos\Delta\theta + I_2 + \frac{\pi}{4}I_{\rm inj}\cos\psi} = \frac{I_1\sin\Delta\theta}{I_1\cos\Delta\theta + I_2}. \tag{28}$$

Equation (28) can be simplified to

$$I_1^2\sin 2\Delta\theta + \frac{\pi}{4}I_{\rm inj}\left[I_1\sin(\psi - \Delta\theta) + I_2\sin\psi\right] = 0. \tag{29}$$

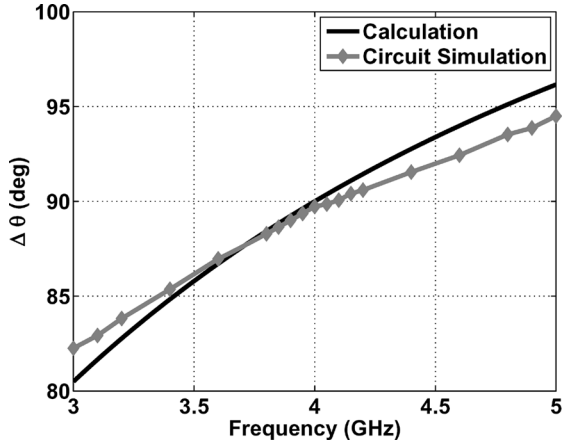

Fig. 4. Circuit-simulated and calculated, using (27), phase differences at the output of a two-stage ring oscillator when an external signal is injected to the output of the first delay cell $f_{\rm SRF} = 4$ GHz.

Using (29), one can find ψ as a function of $\Delta\theta$ and injection current as follows:

$$\psi = \xi - \sin\left(\frac{4}{\pi}\frac{I_1^2\sin 2\Delta\theta}{I_{\rm inj}\sqrt{I_1^2 + I_2^2 + 2I_1I_2\cos\Delta\theta}}\right) \tag{30}$$

where

$$\xi = \tan^{-1}\left(\frac{I_1\sin\Delta\theta}{I_1\cos\Delta\theta + I_2}\right). \tag{31}$$

The smallest required amplitude of injection current to injection-lock the oscillator at $\omega_{\rm inj}$ is obtained from (30)

$$I_{\rm inj} \geq \frac{4}{\pi}\frac{I_1^2|\sin 2\Delta\theta|}{\sqrt{I_1^2 + I_2^2 + 2I_1I_2\cos\Delta\theta}}. \tag{32}$$

Therefore, by substituting $\Delta\theta$ from (27) into (32), one can find a lower bound for $I_{\rm inj}$ to injection-lock the oscillator to $\omega_{\rm inj}$. Last, the solution for ψ is found by substituting the lower bound for $I_{\rm inj}$ into (30).

Repeating this procedure for different values of $\omega_{\rm inj}$ results in the input sensitivity curve ($I_{\rm inj}$ versus $\omega_{\rm inj}$) of the two-stage ring oscillator.

Using this procedure, the calculated locking range of the two-stage ring oscillator is obtained and shown in Fig. 5 and is compared with circuit simulations. It can be seen from Fig. 5 that the error in predicting the minimum injection current at the boundaries of the locking range is less than 6%.

It can be concluded from (16a) and (16b) that, in the presence of any external signal, even if it is at the same frequency as SRF, the amplitudes of the oscillation voltages are not equal. Fig. 6(a) shows the calculated and simulated amplitudes of the output voltages as a function of injection frequency, assuming that the minimum required injection current, from (32), is injected at the output of the first delay cell. As can be observed in Fig. 6(a), the output voltages have equal amplitudes at the SRF. The calculated and simulated amplitude differences versus injection frequency are shown in Fig. 6(b).

Fig. 7(a) shows a graphical representation of the steady-state solution for the oscillation phases of the oscillator in Fig. 3 when

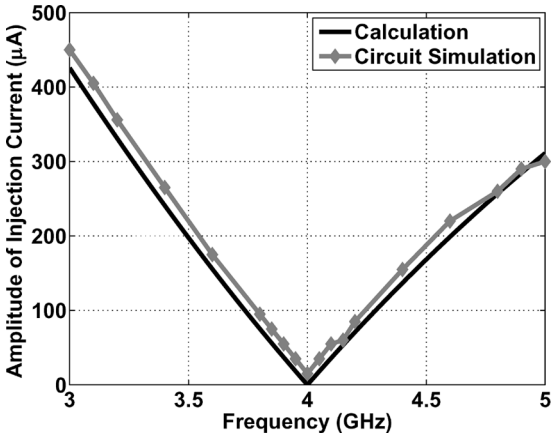

Fig. 5. Calculated, using (32), and circuit-simulated locking ranges of a two-stage ring oscillator when an external signal is injected to the output of the first delay cell.

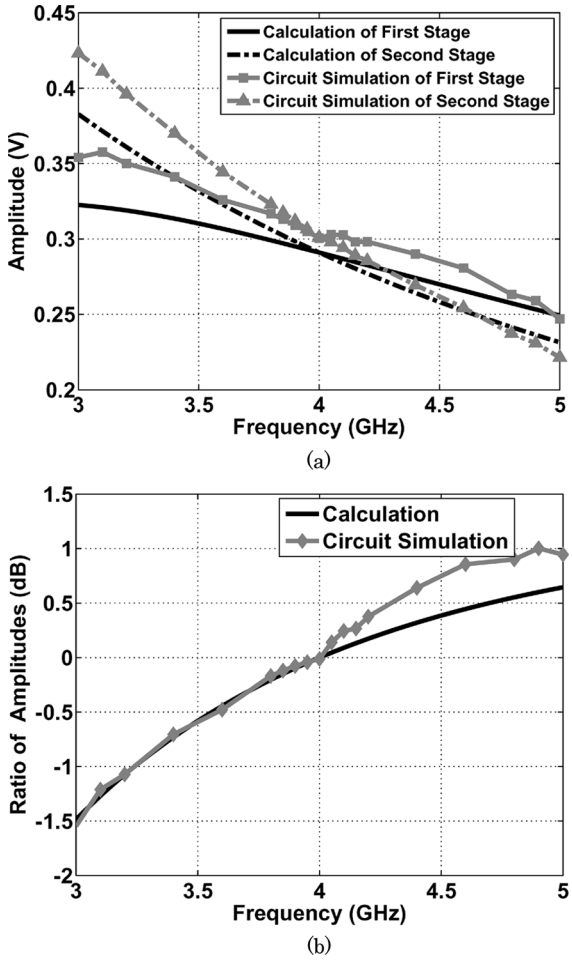

Fig. 6. Amplitudes of oscillation versus injection frequency. (a) Calculated, using (16a) and (16b), and circuit-simulated amplitudes of output voltages and (b) calculated and circuit-simulated amplitude differences when the external signal is injected only at the output of the first delay cell and the minimum required injection current is applied, i.e., $f_{\mathrm{SRF}} = 4\ \mathrm{GHz}$.

it free-runs. In this representation, I_{11} and I_{12} are the corresponding phasors for the I_1 and I_2 current sources of the first delay cell, shown in Fig. 2(b), and I_{21} and I_{22} are the corresponding current phasors of the second delay cell. The resultant currents of the delay cells are denoted by I_{L1} and I_{L2}. As can be seen in Fig. 7(a), when the two-stage ring oscillator free-runs, or locks to its SRF, the two oscillation phases are orthogonal. In this case, the angle between the phasors of the resultant current and the corresponding voltage of each stage is $\phi_0 = \tan^{-1}(I_1/I_2)$.

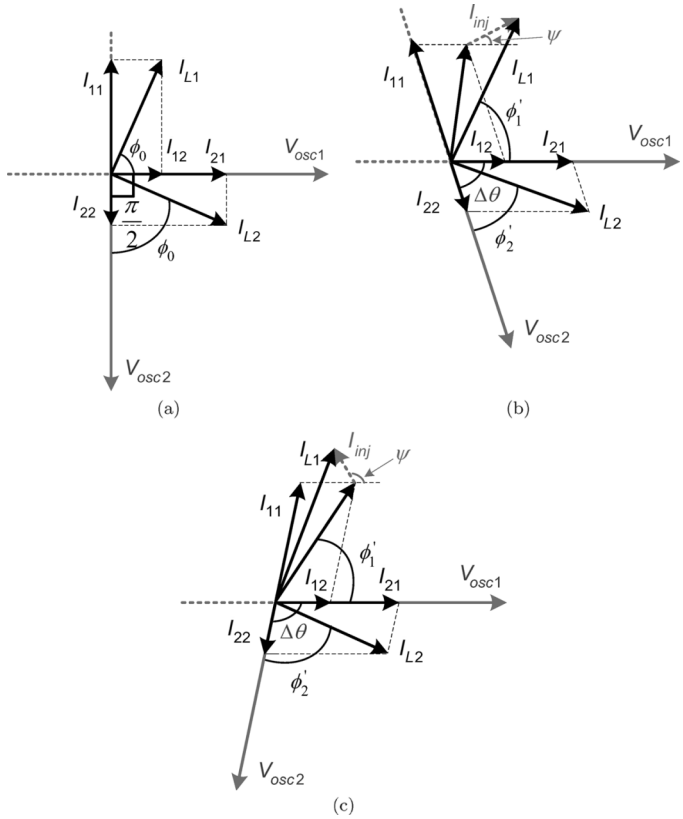

Fig. 7. Graphical representation of steady-state solution for the voltage and current phasors of the two-stage ring oscillator that is (a) free-running, (b) injection-locked to a frequency lower than its SRF, and (c) injection-locked to a frequency greater than its SRF. An external signal is injected at the output of the first delay cell.

Fig. 7(b) shows the same currents and voltages when the oscillator of Fig. 3 is injection-locked to a frequency lower than its SRF. In this case, the phase difference between oscillation phases $\Delta\theta$ is less than $\pi/2$. It can be shown that—in this case—the angle between the phasors of the resultant current and the voltage of each delay cell (ϕ_1' in the first delay cell and ϕ_2' in the second one) is less than ϕ_0. Similarly, Fig. 7(c) shows the voltage and current phasors when the oscillator is injection-locked to a frequency greater than its SRF. In this case, $\Delta\theta$ is greater than $\pi/2$. Similarly, it can be shown that, in this case, ϕ_1' and ϕ_2' are greater than ϕ_0.

The nonquadrature output phases obtained for this scheme of injection-locking when the oscillator is injection-locked to frequencies other than its self-resonance frequencies makes this scheme of injection-locking less attractive for applications with demanding quadrature accuracy. In Section V-C, this oscillator is analyzed when the external signal is injected at the outputs of both delay cells.

C. Two-Stage Ring Oscillator Multinode Injection

In this section, we investigate the two-stage ring oscillator when the external signal is injected to both of its delay cells,

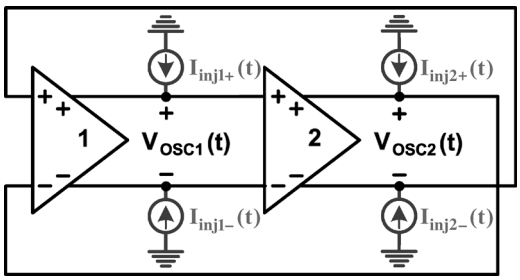

Fig. 8. Two-stage ring oscillator when the external signal is injected at the outputs of both delay cells.

as shown in Fig. 8. There are several reasons for injecting the external signal at multiple nodes instead of a single node.

1) It provides balanced loading for the previous stage in differential circuits.
2) It may increase the locking range of the oscillator under injection, as shown in [15] and [16].
3) In this problem, it may help to maintain quadrature phases ($\Delta\theta = \pi/2$) and equal amplitudes for the fundamental harmonics of output voltages in the entire locking range.

In this section, we propose a technique to maintain $\Delta\theta = \pi/2$ for the entire locking range of the oscillator.

Using similar assumptions and procedures that were used to derive (12) and (13), the following set of differential equations are derived for the amplitudes and phases of the oscillator when external signals are injected to the outputs of both delay cells (Fig. 8)

$$\frac{V1_1}{R} + jCV1_1\frac{\mathrm{d}\theta_{1,1}(t)}{\mathrm{d}t} = -\frac{2I_1}{\pi}\mathrm{e}^{j[\theta_{2,1}(t)-\theta_{1,1}(t)]} + \frac{2I_2}{\pi} + \frac{1}{2}I_{\mathrm{inj1}}\mathrm{e}^{j[\theta_{\mathrm{inj1}}(t)-\theta_{1,1}(t)]} \quad (33a)$$

$$\frac{V2_1}{R} + jCV2_1\frac{\mathrm{d}\theta_{2,1}(t)}{\mathrm{d}t} = \frac{2I_1}{\pi}\mathrm{e}^{j[\theta_{1,1}(t)-\theta_{2,1}(t)]} + \frac{2I_2}{\pi} + \frac{1}{2}I_{\mathrm{inj2}}\mathrm{e}^{j[\theta_{\mathrm{inj2}}(t)-\theta_{2,1}(t)]}. \quad (33b)$$

Separating the real and imaginary parts of (33a) and (33b) will result in differential equations that relate the amplitudes and phases of the fundamental harmonic of the output voltages to the amplitudes and phases of the injection signals. One can use (14a) and the following definitions to simplify the results:

$$\psi_1 \triangleq \theta_{\mathrm{inj1}}(t) - \theta_{1,1}(t) \quad (34a)$$

$$\psi_2 \triangleq \theta_{\mathrm{inj2}}(t) - \theta_{2,1}(t) \quad (34b)$$

resulting in

$$\frac{\mathrm{d}\theta_{1,1}(t)}{\mathrm{d}t} = \frac{1}{RC}\frac{I_1\sin\Delta\theta + \frac{\pi}{4}I_{\mathrm{inj1}}\sin\psi_1}{-I_1\cos\Delta\theta + I_2 + \frac{\pi}{4}I_{\mathrm{inj1}}\cos\psi_1} \quad (35a)$$

$$\frac{\mathrm{d}\theta_{2,1}(t)}{\mathrm{d}t} = \frac{1}{RC}\frac{I_1\sin\Delta\theta + \frac{\pi}{4}I_{\mathrm{inj2}}\sin\psi_2}{I_1\cos\Delta\theta + I_2 + \frac{\pi}{4}I_{\mathrm{inj2}}\cos\psi_2}. \quad (35b)$$

In addition, the steady-state amplitudes of the fundamental harmonics of the output voltages are obtained from (33a) and (33b)

$$V_{a1} = R\left(-\frac{4I_1}{\pi}\cos\Delta\theta + \frac{4I_2}{\pi} + I_{\mathrm{inj1}}\cos\psi_1\right) \quad (36a)$$

$$V_{a2} = R\left(\frac{4I_1}{\pi}\cos\Delta\theta + \frac{4I_2}{\pi} + I_{\mathrm{inj2}}\cos\psi_2\right). \quad (36b)$$

To complete the analysis, we also assume that the external signals that are used to injection-lock the oscillator have equal amplitudes, i.e., $I_{\mathrm{inj1}} = I_{\mathrm{inj2}} = I_{\mathrm{inj}}$. From (22), (35a), and (35b), it is concluded that, in steady state, the following relation between ψ_1, ψ_2, $\Delta\theta$, and I_{inj} holds:

$$\frac{I_1\sin\Delta\theta + \frac{\pi}{4}I_{\mathrm{inj}}\sin\psi_1}{-I_1\cos\Delta\theta + I_2 + \frac{\pi}{4}I_{\mathrm{inj}}\cos\psi_1} = \frac{I_1\sin\Delta\theta + \frac{\pi}{4}I_{\mathrm{inj}}\sin\psi_2}{I_1\cos\Delta\theta + I_2 + \frac{\pi}{4}I_{\mathrm{inj}}\cos\psi_2}. \quad (37)$$

We need to find a solution for (37) that satisfies $\Delta\theta = \pi/2$ for every value of I_{inj}, ψ_1, and ψ_2. By substituting $\Delta\theta = \pi/2$ into (37), we obtain the following:

$$\sin\left(\frac{\psi_1-\psi_2}{2}\right)\left[2I_1\sin\left(\frac{\psi_1+\psi_2}{2}\right) + 2I_2\cos\left(\frac{\psi_1+\psi_2}{2}\right) + \frac{\pi}{2}I_{\mathrm{inj}}\cos\left(\frac{\psi_1-\psi_2}{2}\right)\right] = 0. \quad (38)$$

By inspection, we can see that $\psi_1 = \psi_2$ satisfies (38) for all the values of I_{inj}. If we define $\Delta\theta_{\mathrm{inj}}$ as $\theta_{\mathrm{inj1}} - \theta_{\mathrm{inj2}}$, it can be shown that, to have quadrature output phases in the oscillator in Fig. 8, the following condition needs to be true:

$$\Delta\theta_{\mathrm{inj}} = \pi/2. \quad (39)$$

To provide quadrature inputs for this scheme of injection-locking, one can use a polyphase filter or supply these phases using another ring oscillator. However, when the ring oscillator in Fig. 8 is used as a divide-by-two frequency divider, the external signal is applied to the gate of the tail current source $MT1$ of the delay cell shown in Fig. 2(b). Since this signal is at a frequency twice the ω_{SRF}, the external signals applied to the gate terminals of the tail current sources in delay cells need to be 180 ° out of phase to satisfy (39). This simplifies the problem of providing the oscillator under locking with the appropriate phases of external signal. Moreover, in this case, the oscillator/frequency divider can provide balanced loading for its preceding differential stage. It is particularly of practical interest in injection-locked regenerative frequency dividers where the oscillator is driven by a differential SSB mixer.

By substituting the solution to (38), i.e., $\psi_1 = \psi_2 = \psi$, into (37), one can find an expression for the oscillation frequency under injection-locking in terms of the circuit parameters and the amplitudes and phases of the external signals

$$\omega_{\mathrm{inj}} = \omega_{\mathrm{SRF}}\left(\frac{1+\gamma\sin\psi}{1+\delta\cos\psi}\right) \quad (40)$$

where

$$\gamma = \frac{\pi}{4}\frac{I_{\rm inj}}{I_1} \tag{41a}$$

$$\delta = \frac{\pi}{4}\frac{I_{\rm inj}}{I_2}. \tag{41b}$$

A comparison with the case where the external signal is only injected to the first delay cell reveals that the oscillation frequency of the multinode injection case is modulated by the angle between the injection current and the oscillation voltage (ψ), as shown in (40), while $\Delta\theta$ modulates the oscillation frequency in the single-injection case, as shown in (24).

If $\omega_{\rm inj}$ is in the locking range of the oscillator, ψ can be determined by

$$\psi = \sin^{-1}\left(\frac{\omega_{\rm inj}/\omega_{\rm SRF} - 1}{\gamma\sqrt{1+(RC\omega_{\rm inj})^2}}\right) - \tan^{-1}(RC\omega_{\rm inj}). \tag{42}$$

The minimum required injection current to injection-lock the two-stage ring oscillator to $\omega_{\rm inj}$ is obtained from (42) and (19)

$$I_{\rm inj} \geq \frac{4}{\pi}\frac{I_1}{\sqrt{1+\left(\frac{I_1}{I_2}\frac{\omega_{\rm inj}}{\omega_{\rm SRF}}\right)^2}}\left|\frac{\omega_{\rm inj}}{\omega_{\rm SRF}} - 1\right|. \tag{43}$$

Using (43), one can obtain the locking range of the two-stage ring oscillator when an injection current is injected to both delay cells. The calculated and simulated locking ranges of the two-stage ring oscillator are shown in Fig. 9.

As can be seen from this figure, the calculation and simulations match within the locking range. They deviate at the high end of the locking range, and the maximum error at 6.2 GHz is approximately 20%, due to additional parasitic components that are not included in the model of the injection-locked frequency divider (ILFD).

This simulated locking range is compared with the simulated locking range from Section V-B where the external signal was only applied to the first delay cell. The result versus the normalized injection current amplitude is shown in Fig. 10. It is observed from this plot that applying the external signal to both the delay cells, with appropriate phase sequences and equal amplitudes, leads to a wider locking range and hence improves the sensitivity of the injection-locked oscillator. This result is in agreement with what was obtained in [15] and [16] for ring oscillators with more than three stages.

An output phase difference $(\Delta\theta)$ of $\pi/2$ between fundamental harmonics of the output voltages is expected for this scheme of injection-locking, and the circuit simulations agree with that.

Note that, under these assumptions, the amplitudes of the output voltages remain equal for all the values of injection frequency within the locking range of the oscillator and are expressed by

$$V_{a1} = V_{a2} = R\left(\frac{4I_2}{\pi} + I_{\rm inj}\cos\psi\right). \tag{44}$$

The calculated and simulated amplitudes of the fundamental component of the output voltages are shown in Fig. 11. It is expected from (44) that, for this scheme of injection-locking, the amplitudes of the output voltages remain equal within the locking range of the two-stage ring oscillator, and this is confirmed in circuit simulations.

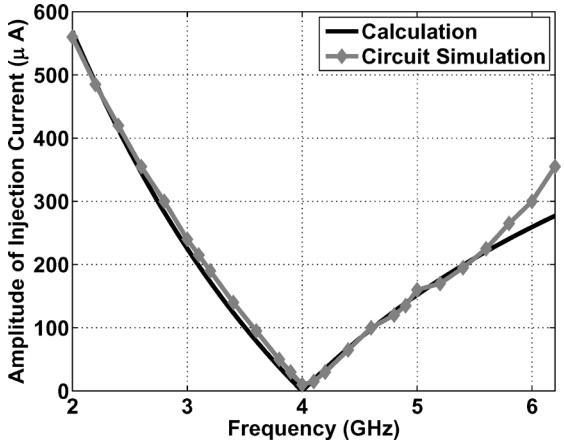

Fig. 9. Calculated, using (43), and circuit-simulated locking ranges of a two-stage ring oscillator when external signals are injected at the outputs of both delay cells.

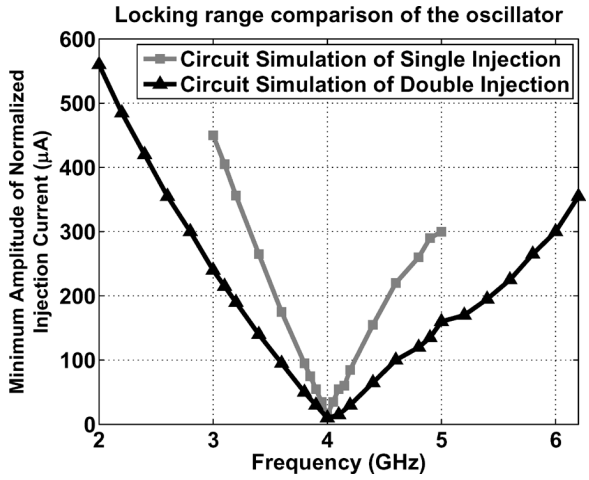

Fig. 10. Circuit-simulated locking range of a two-stage ring oscillator, $f_{\rm SRF} = 4$ GHz for different injection-locking schemes.

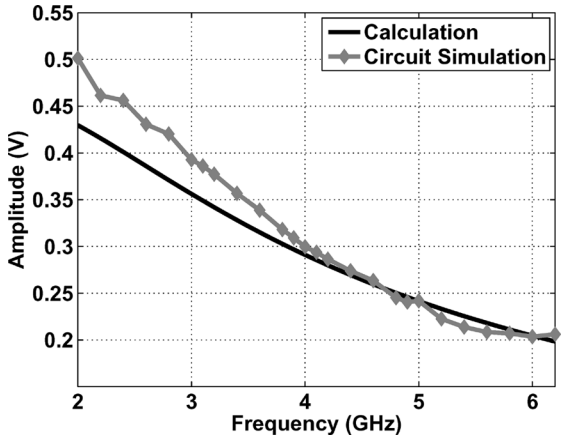

Fig. 11. Calculated, using (44), and circuit-simulated amplitudes of output voltages versus injection frequency.

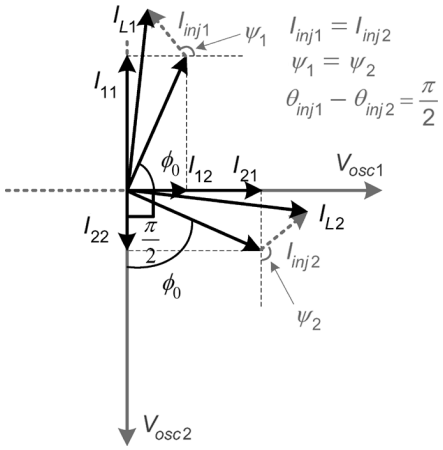

Fig. 12. Graphical representation of steady-state solution for the voltage and current phasors of the two-stage ring oscillator when external signals are injected to both delay cells with equal amplitudes and quadrature phases.

Fig. 12 shows a graphical representation of the steady-state solution for the phasors of the voltages and currents of the oscillator in Fig. 8 when external signals are injected to both delay cells. It can be seen that, under the constraints derived for external signals ($I_{\rm inj1} = I_{\rm inj2}$ and $\Delta\theta_{\rm inj} = \pi/2$), the oscillation voltages remain in quadrature with equal amplitudes. Similar to Fig. 7(a), I_{11} and I_{12} are the corresponding phasors for the I_1 and I_2 current sources [Fig. 2(a)] of the first delay cell, I_{21} and I_{22} are the corresponding current phasors to the second delay cell, and I_{L1} and I_{L2} are the resultant currents of the first and second delay cells, respectively.

Circuit simulations across the locking range show that a 20% input amplitude mismatch leads to quadrature amplitude and phase mismatches of 0.4 dB and 2 ° at the output of the ring oscillator in Fig. 8. In this case, the amplitudes of the injection currents injected to the outputs of the delay cells in Fig. 8 are 605 and 495 μA. On the other hand, an input phase mismatch of $\pm 5°$ leads to output amplitude and phase mismatches of 0.4 dB and 0.5 °, respectively. The injection-locked oscillator draws 4 mA from a 1.2-V supply across the locking range. It can be shown that if the input amplitude mismatch is negligible, an input phase mismatch of ε causes an output phase mismatch of

$$\theta_{\rm mm} \approx \frac{\pi}{4}\frac{I_{\rm inj}}{I_1^2}(I_1 \sin\psi + I_2 \cos\psi)\sin\varepsilon \tag{45}$$

where I_1 and I_2 are the bias currents of the negative-resistance delay cell in Fig. 2(b). In the derivation of (45), it is assumed that $\varepsilon \leq 10°$.

VI. Phase-Noise Analysis of Injection-Locked Regenerative Divider

To analyze the output phase noise of the injection-locked regenerative frequency divider, we use the simplified block diagram of this divider with the main phase-noise sources shown in Fig. 13. It is assumed that the oscillator's internal phase noise and the phase noise of the input frequency to the divider are the main contributors to the output phase noise.

To start the analysis, we assume that steady state is reached and the oscillator is superharmonic injection-locked to the Rth harmonic of its output frequency.

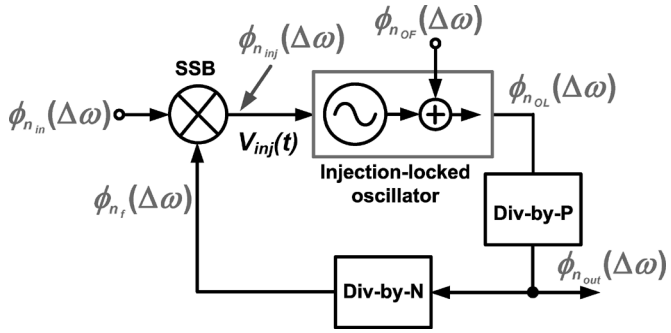

Fig. 13. Phase-noise mechanism in an injection-locked regenerative frequency divider.

It is shown in [18] that a superharmonic injection-locked oscillator to the Rth harmonic of its output frequency behaves like a first-order phase-locked loop with an input-phase-to-output-phase transfer function of $G(S) = 1/(1 + S/\omega_P)$, where $S = j\Delta\omega$ and, as shown in [1], ω_P for the injection-locked oscillator in Fig. 8 is approximately

$$\omega_P = \frac{\frac{\pi}{4} I_{\rm inj}\cos\psi}{I_1 + \frac{\pi}{4} I_{\rm inj}\sin\psi}\omega_{\rm inj}. \tag{46}$$

Consequently, the phase noise at the output of the injection-locked oscillator $[\overline{\phi^2_{n\rm OL}}(\Delta\omega)]$ can be expressed in terms of the oscillator's intrinsic noise $[\overline{\phi^2_{n\rm OF}}(\Delta\omega)]$ and the phase noise of the injection signal $[\overline{\phi^2_{n\rm inj}}(\Delta\omega)]$

$$\overline{\phi^2_{n\rm OL}}(\Delta\omega) = \frac{1}{R^2}\frac{1}{1+(\Delta\omega/\omega_P)^2}\overline{\phi^2_{n\rm inj}}(\Delta\omega) + \frac{(\Delta\omega/\omega_P)^2}{1+(\Delta\omega/\omega_P)^2}\overline{\phi^2_{n\rm OF}}(\Delta\omega). \tag{47}$$

As can be seen from (47), the phase noise at the output of the oscillator consists of two components: the oscillator's intrinsic phase noise, which goes through a first-order high-pass transfer function, and the phase noise of the injection signal, which encounters a first-order low-pass transfer function. Consequently, the close-in phase noise of the injection-locked oscillator is dominated by the phase noise of the injection signal, while the high-frequency phase noise follows the internal phase noise of the free-running oscillator. Therefore, $\overline{\phi^2_{n\rm OL}}(\Delta\omega)$ can be approximated for close-in phase ($\Delta\omega \ll \omega_P$) and high-frequency phase noise ($\Delta\omega \gg \omega_P$) by

$$\overline{\phi^2_{n\rm OL}}(\Delta\omega) \approx \begin{cases} \frac{1}{R^2}\overline{\phi^2_{n\rm inj}}(\Delta\omega), & \Delta\omega \ll \omega_P \\ \overline{\phi^2_{n\rm OF}}(\Delta\omega), & \Delta\omega \gg \omega_P. \end{cases} \tag{48}$$

As discussed in [19], if the SSB phase noise of the inputs to the mixer of Fig. 1(c) are $\overline{\phi^2_{n\rm in}}$ and $\overline{\phi^2_{nf}}$ and if the amplitude of the signal at the mixer output is sufficiently large, the output phase noise of the mixer is mainly dominated by the phase noise of the inputs and can be written as

$$\overline{\phi^2_{n\rm inj}}(\Delta\omega) = \overline{\phi^2_{n\rm in}}(\Delta\omega) + \overline{\phi^2_{nf}}(\Delta\omega). \tag{49}$$

Since the divide-by- P is locked to the oscillator output, we can assume that its output phase noise is dominated by the phase noise of the injection-locked oscillator, i.e.,

$\overline{\phi^2_{n\text{out}}}(\Delta\omega) = \overline{\phi^2_{n\text{OL}}}(\Delta\omega)/P^2$. As a result, the phase noise of the feedback signal (the output of the divide-by- N) is

$$\overline{\phi^2_{nf}}(\Delta\omega) = \overline{\phi^2_{n\text{OL}}}(\Delta\omega)/(NP)^2. \tag{50}$$

Substituting (49) and (50) into (48), the output phase noise of the injection-locked regenerative divider $\pounds_{\text{out}}\{\Delta\omega\} = 10\log[\overline{\phi^2_{n\text{out}}}(\Delta\omega)]$ can be expressed as

$$\pounds_{\text{out}}\{\Delta\omega\} \approx \begin{cases} 10\log\left[\frac{\overline{\phi^2_{n\text{in}}}(\Delta\omega)}{(RP)^2-1/N^2}\right], & \Delta\omega \ll \omega_P \\ 10\log\left[\frac{\overline{\phi^2_{n\text{OF}}}(\Delta\omega)}{P^2}\right], & \Delta\omega \gg \omega_P. \end{cases} \tag{51}$$

It can be concluded from (47) that if the injection signal is noiseless, the phase noise at the output of the frequency divider would be equal to the attenuated extrinsic phase noise of the oscillator [15], [18]; in other words

$$\pounds_{\text{out}}\{\Delta\omega\} = 10\log\left[\frac{(\Delta\omega/\omega_P)^2}{1+(\Delta\omega/\omega_P)^2}\frac{\overline{\phi^2_{n\text{OF}}}(\Delta\omega)}{P^2}\right]. \tag{52}$$

To complete this section, we investigate the phase noise of the two-stage ring oscillator in Fig. 2(a). The free-running phase noise of a two-stage ring-oscillator-based VCO that uses negative-resistance delay cells with active loads is calculated in [20] using the impulse sensitivity function technique of [21] and [22]. Here, we use the result obtained in [20] to find the phase noise of the two-stage ring oscillator in Fig. 2. In this case, the free-running phase noise at the offset $\Delta\omega$ from the carrier (in dBc/Hz) can be expressed as

$$\pounds_{\text{FR}}\{\Delta\omega\} = 10\log\left[\frac{\pi^2}{24}\frac{\left(\overline{i_n^2}\Big/\Delta f\right)}{(CV_{\text{sw}})^2(\Delta\omega)^2}\right] \tag{53}$$

where $\overline{i_n^2}/\Delta f$ is the output referred mean square current noise density which contains both thermal and flicker noises and can be expressed by $\overline{i_n^2}(M1,M2,M3,M4)/\Delta f + 2\times 4kT/R_L$. In this expression, R_L is the load resistor used in the delay cell in Fig. 2(b) since it is the only noisy component of the output resistance at the output of each delay cell. Using the oscillation frequency given by (19), the phase noise (53) can be rewritten as

$$\pounds_{\text{FR}}\{\Delta\omega\} = 10\log\left[\frac{\pi^2}{24}\left(\frac{RI_2}{V_{\text{sw}}I_1}\right)^2\frac{\left(\overline{i_n^2}\Big/\Delta f\right)}{(\Delta\omega/\omega_{\text{SRF}})^2}\right]. \tag{54}$$

The simulated and calculated free-running phase noise of the prototype two-stage ring oscillator from Section V-B is shown in Fig. 14(a). To precisely calculate the phase noise, $\overline{i_n^2}/\Delta f$ is measured using circuit simulation and then substituted into (54). The simulated injection-locked phase noise of this two-stage ring oscillator for different amplitudes of the injection signal is shown in Fig. 14(b). To obtain these plots, this two-stage ring oscillator is used as a divide-by-two, and noiseless differential injection signals are applied to the gates of transistors labeled by $MT1$ [Fig. 2(b)] in each delay cell. As was discussed before, the output phase noise of the oscillator is its attenuated internal noise, and this noise is more attenuated for larger amplitudes of injection signals.

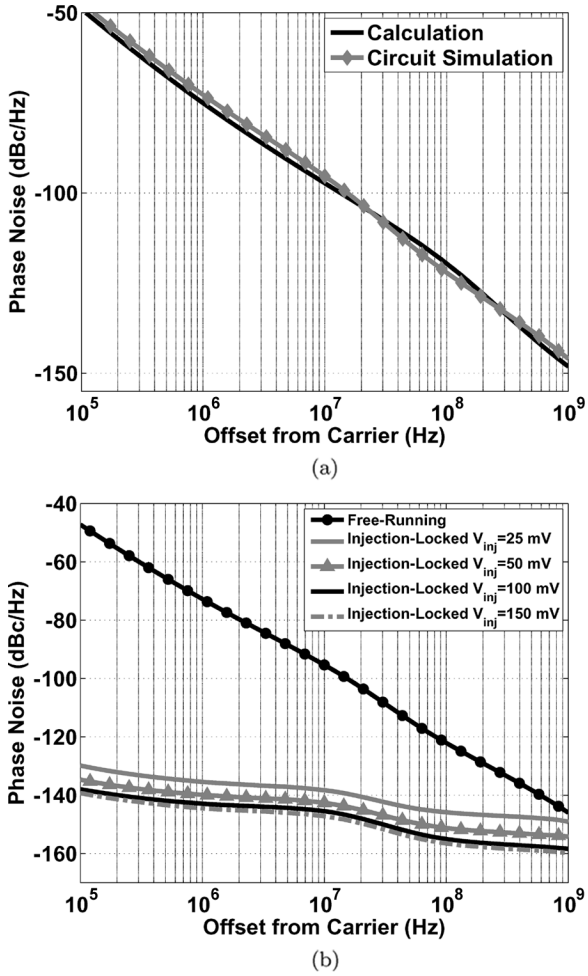

Fig. 14. Phase noise of the prototype two-stage ring oscillator. (a) Calculated phase noise from (54) versus circuit simulation of free-running phase noise and (b) circuit-simulated phase noise when injection-locked to a noiseless injection signal for different values of injection signals (an external signal is injected to both delay cells).

Using (51), (54), and the phase noise of the injection signal, one can calculate the output phase noise of the injection-locked regenerative frequency divider.

VII. Design Example of a Divide-by-2.25/4.5

As mentioned earlier, one of the benefits of the injection-locked regenerative frequency divider is its ability to obtain fractional division ratios while providing 50% duty-cycle quadrature output phases. In this section, we present a design example of an injection-locked regenerative frequency divider that generates a fractional division ratio.

One of the design goals is to achieve a design suitable for implementation in a digital CMOS submicrometer technology using no on-chip inductor. This goal implies using ring oscillators with resistive loads and also exploiting SSB mixers in the injection-locked regenerative frequency divider. The latter requires the availability of the quadrature phases of both the input to the frequency divider and its output or, more precisely, the output of the feedback path.

There are several ways to provide the quadrature phases of input, such as using polyphase filters or preceding the divide-by-2.25 by another frequency divider or a ring oscillator that can generate quadrature output phases. As previously

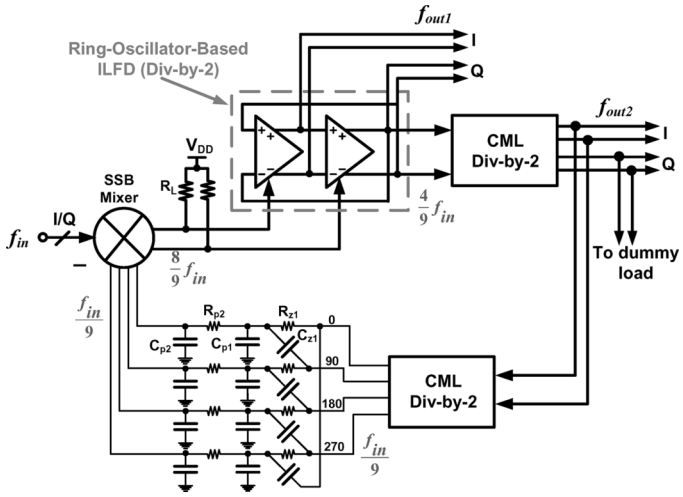

Fig. 15. Simplified schematic of a divide-by-2.25/4.5 with quadrature outputs and 50% duty cycle using an injection-locked regenerative frequency divider architecture. An SSB mixer based on Gilbert cell mixer with resistive load is used. Dummy loads at the output of frequency dividers are not shown.

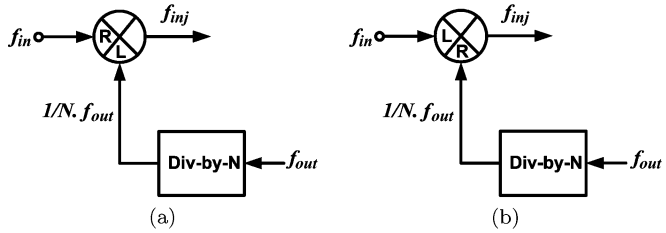

Fig. 16. Block diagrams of the injection-locked regenerative frequency dividers with quadrature outputs and 50% duty cycle (a) with a fractional division ratio (2.25 and 4.5) and (b) with integer division ratio (divide-by-three).

stated, a block with quadrature outputs in the forward path is required to generate quadrature output phases. A divide-by-two flip-flop is usually a good candidate for this purpose, since most divide-by-two circuits can provide quadrature output phases. On the other hand, any oscillator that is injection-locked to its second harmonic can be used as a divide-by-two. Two-stage, or four-stage, ring oscillators are good examples that serve as divide-by-two circuits and provide quadrature outputs.

Fig. 15 shows a fractional frequency divider based on the general architecture in Fig. 1(c). This frequency divider is primarily designed to obtain a division ratio of 2.25 to be used for frequency synthesis for multiband orthogonal frequency-division multiplexing ultrawideband [1]. The ILFD in the forward path of the frequency divider in Fig. 15 is implemented using the two-stage ring oscillator with negative-resistance delay cells shown in Fig. 2. In addition to operating with a smaller input drive, an ILFD can operate at higher speeds in comparison to static frequency dividers. The feedback path of the frequency divider in Fig. 15 consists of a cascade of two flip-flop-based CML divide-by-two circuits. Using divide-by-two blocks in the feedback path provides quadrature phases for the operation of the SSB mixer.

From (1), it can be concluded that, in the steady state, $f_{\rm out1} = f_{\rm in}/2.25$ and $f_{\rm out2} = f_{\rm in}/4.5$. Therefore, the frequency divider in Fig. 15 achieves division ratios of both 2.25 and 4.5. In contrast to the previous approaches [3], no on-chip inductor is required to implement this frequency divider.

As mentioned in Section V-C, when appropriate injection signals are applied to both the delay cells of the ring oscillator in Fig. 2, there is no systematic quadrature mismatch at the output. Monte Carlo simulation using the extracted layout of the frequency divider was performed to investigate the quadrature output mismatches induced by process variations, device mismatches, and layout imperfections. The simulation results showed a standard deviation of 0.3 dB for quadrature amplitude mismatch and a standard deviation of 1.4 ° for quadrature phase error across the locking range. These amplitude and phase mismatches are tolerable for most applications. The frequency divider in Fig. 15 and its output buffers (not shown in Fig. 15) draw 14 mA from a 1.2-V supply.

The frequency divider in Fig. 15 is similar to the divide-by-4.5 presented in [23] where the forward path consists of a cascade of two divide-by-two and the feedback path is implemented using a divide-by-two. The first divide-by-two in the forward path is a CML divider, and the other two frequency dividers are implemented using true single-phase clocked logic [24] to reduce the power dissipation. The SSB mixer in [23] uses an inductive load to suppress unwanted mixing products. The frequency divider of [23] does not use any linearization technique or harmonics polyphase filtering used in the frequency divider in Fig. 15.

The input signal to the frequency divider can be applied to either the RF port (Gm stage) or the LO port of the SSB mixer. When it is connected to the RF port, as shown in Fig. 16(a), the divider achieves a better input sensitivity; thus, it can function with smaller input power. On the other hand, the output of the feedback path frequency divider is fed to the LO port. The large swing of the CML divider output is suitable for the saturation operation of the LO port of the mixer. However, in this case, all the odd harmonics of the feedback signal contribute to in-band mixing products at the mixer output since the feedback signal is at a lower frequency than the input signal. Consequently, the signal at the output of the mixer can achieve a non-50% duty cycle which leads to the I/Q phase inaccuracy at the final output of the main frequency divider. Moreover, as shown in [25], any frequency spur at the input of a divide-by-two translates to a spur at the output of the divider at the same offset frequency.

To solve these issues, one can use the scheme shown in Fig. 16(b) in which the input signal, which is at a greater frequency than the feedback signal, is applied to the LO port of the SSB mixer. In this scheme, the feedback signal is applied to the RF port (Gm stage) of the mixer. The contribution of the feedback signal to higher order in-band mixing products can be minimized by linearizing the Gm stage of the mixer. In addition, the feedback signal, which is rich in harmonics, can go through harmonic suppression filtering. In the presence of the quadrature phases of the feedback signal, a polyphase filter can be used since, first, it provides balanced loading for all the outputs of the feedback frequency divider, second, it can achieve better harmonic suppression by generating imaginary zeros, and third, it does not require any on-chip inductor or balun. The drawback of the scheme shown in Fig. 16(b) is the degraded input sensitivity of the resultant frequency divider.

In this scheme, if the input signal is smaller than required for the saturation operation of the mixer LO port, the amplitude of the mixer output signal depends on the input amplitude and, hence, could be small. As previously stated, using an ILFD in the forward path of the divide-by-2.25 has the advantage that it can operate with smaller input drive. As a result, it can guarantee

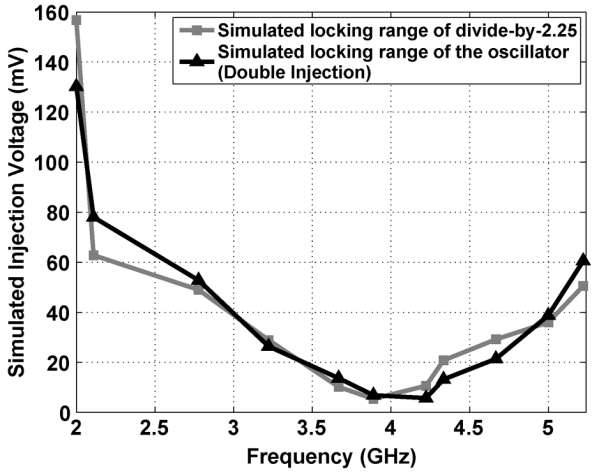

Fig. 17. Circuit-simulated locking range of the prototype divide-by-2.25/4.5 and comparison with the locking range of the oscillator used in it.

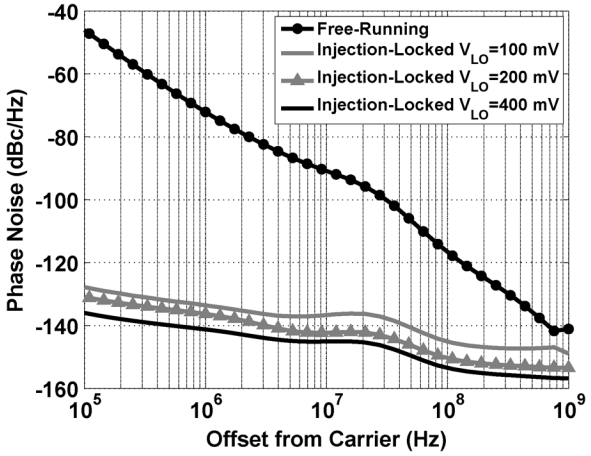

Fig. 18. Circuit simulation of free-running and injection-locked phase noise of the prototype divide-by-2.25/4.5 for different LO amplitudes.

the robust operation of the injection-locked regenerative divider in Fig. 15.

As was discussed in Section IV, the choice of this ILFD, or generally, the forward path oscillator, is directly tied to the stability of the injection-locked regenerative divider. Nonetheless, using an ILFD mandates careful analysis and simulations to make sure that it has a wide-enough locking range to compensate for process variations. A ring-oscillator-based ILFD has wider locking range compared with the LC oscillator. In addition, it can provide multiple phases of output, occupies smaller area on silicon, and is more compatible with the digital CMOS technology.

As was shown in Section IV, the locking range of the injection-locked regenerative divider follows the locking range of its oscillator. The input to the RF port of the mixer (Fig. 15) is set by the output of its preceding frequency divider. Therefore, in order to control the amplitude of $V_{\rm inj}(t)$, the amplitude of the input to the LO port of the mixer is varied. The simulated locking range of this divider is shown in Fig. 17 and is compared with the locking range of the two-stage negative-resistance-based ring oscillator. As can be seen, the agreement is very good throughout the locking range, and the maximum error in predicting the injection voltage is about 30 mV at the low end of the locking range.

Fig. 18 shows the simulated free-running and locked phase noise of the frequency divider for an output frequency of 4 GHz when a noiseless input signal is input to the divider. The amplitude of the injection signal is changed by changing the amplitude of the input to the LO port of the mixer. From (52), we expect to obtain a similar output phase noise to those in Fig. 14, and comparing Fig. 18 and 14 shows a very good agreement within 2 dB.

VIII. Conclusion

This paper has presented an analysis of the operation, stability, locking range, and phase noise of injection-locked regenerative frequency dividers. In addition, the injection-locked behavior of two-stage ring oscillators (based on negative-resistance delay cells) is studied, and their locking range is derived for the first time. Finally, a design technique was presented for implementing a regenerative frequency divider in a digital CMOS technology (using no on-chip inductor or balun) for achieving fractional division ratios with 50% duty-cycle quadrature output phases. The circuit simulation results of the designed oscillator and the fractional injection-locked regenerative frequency divider are in excellent agreement with the calculations.

Appendix A
Derivation of Voltage and Phase Relationships in an Injection-Locked Two-Stage Ring Oscillator

If the values of $V_{\rm OSC1}(t)$ and $V_{\rm OSC2}(t)$ are sufficiently large, the transistors of each delay cell in Fig. 2(a) are fully switched and the current waveforms of $I_{D1}(t) - I_{D2}(t)$ and $I_{D3}(t) - I_{D4}(t)$ are similar to a ± 1 square wave. These waveforms are in phase with the fundamental component of their controlling voltages [15], i.e., $I_{D1}(t) - I_{D2}(t)$ in the first delay cell is in phase with the fundamental harmonic of $-V_{\rm OSC2}(t)$ and $I_{D3}(t) - I_{D4}(t)$ is in phase with the fundamental harmonic of $V_{\rm OSC1}(t)$; thus, they can be represented using a Fourier series as follows:

$$[I_{D1}(t) - I_{D2}(t)] = \sum_{k=-\infty}^{+\infty} I1_{(2k-1)} e^{j[(2k-1)\theta_{2,1}(t)-\pi]} \quad (55a)$$

$$[I_{D3}(t) - I_{D4}(t)] = \sum_{k=-\infty}^{+\infty} I2_{(2k-1)} e^{j(2k-1)\theta_{1,1}(t)}. \quad (55b)$$

The factor $-\pi$ in the argument of the instantaneous phase of $I_{D1}(t) - I_{D2}(t)$ in (55a) comes from its controlling voltage, which is the fundamental harmonic of $-V_{\rm OSC2}(t)$. To represent a real current, $Ij_{(2k-1)}$ and $Ij_{-(2k-1)}$ must be complex conjugates ($j = 1, 2$). As shown in [26], under the stated assumptions, $I1_1$ and $I2_1$ are $2I_1/\pi$ and $2I_2/\pi$, respectively. We also assume that the differential injection current can be represented by $I_{\rm inj}\cos(\theta_{\rm inj}(t))$, where $\theta_{\rm inj} = \omega_{\rm inj}t + \phi_{\rm inj}$. By substituting (10a), (10b), (55a), and (55b) into (8) and considering the stabilized amplitude of oscillation under steady state, the following was achieved:

$$\sum_{k=-\infty}^{+\infty} \frac{V1_{(2k-1)}}{R} e^{j\theta_{1,(2k-1)}(t)} + jC\left(\sum_{k=-\infty}^{+\infty} V1_{(2k-1)} \frac{\rm d}{{\rm d}t}\left[\theta_{1,(2k-1)}(t)\right] e^{j\theta_{1,(2k-1)}(t)}\right)$$

$$= -\sum_{k=-\infty}^{+\infty} I1_{(2k-1)} e^{j(2k-1)\theta_{2,1}(t)} + \sum_{k=-\infty}^{+\infty} I2_{(2k-1)} e^{j(2k-1)\theta_{1,1}(t)} + I_{\text{inj}} \cos\theta_{\text{inj}}. \quad (56)$$

When the oscillator is injection-locked, $\omega_o = \omega_{\text{inj}}$. Equating the coefficients of similar exponents in (56) results in the following where $\delta_{(2k-1),\pm 1}$ is the Kronecker delta and equals one for the fundamental harmonic of output voltages ($k = 0, 1$) and is zero for other harmonics:

$$\frac{V1_{(2k-1)}}{R} e^{j\theta_{1,(2k-1)}(t)} + jCV1_{(2k-1)} \frac{\mathrm{d}}{\mathrm{d}t}\left[\theta_{1,(2k-1)}(t)\right] e^{j\theta_{1,(2k-1)}(t)} = -I1_{(2k-1)} e^{j(2k-1)\theta_{2,1}(t)} + I2_{(2k-1)} e^{j(2k-1)\theta_{1,1}(t)} + \frac{1}{2} I_{\text{inj}} e^{j\theta_{\text{inj}}(t)} \delta_{(2k-1),\pm 1}, \qquad k \in \mathbb{Z}. \quad (57)$$

The harmonics of the currents of (55a) and (55b) have a roll-off of approximately $1/|2k-1|$. Moreover, these harmonics go through the low-pass filter of the output load of each delay cell. As a result, the fundamental harmonic is dominant.

Substituting $k = 1$ into (57) results in a differential equation for the fundamental harmonic of $V_{\text{OSC1}}(t)$

$$\frac{V1_1}{R} e^{j\theta_{1,1}(t)} + jCV1_1 \frac{\mathrm{d}\theta_{1,1}(t)}{\mathrm{d}t} e^{j\theta_{1,1}(t)} = -I1_1 e^{j\theta_{2,1}(t)} + I2_1 e^{j\theta_{1,1}(t)} + \frac{1}{2} I_{\text{inj}} e^{j\theta_{\text{inj}}(t)}. \quad (58)$$

After substituting the values of $I1_1$ and $I2_1$ into (58), it can be rewritten as

$$\frac{V1_1}{R} + jCV1_1 \frac{\mathrm{d}\theta_{1,1}(t)}{\mathrm{d}t} = -\frac{2I_1}{\pi} e^{j[\theta_{2,1}(t) - \theta_{1,1}(t)]} + \frac{2I_2}{\pi} + \frac{1}{2} Iq_{\text{inj}} e^{j[\theta_{\text{inj}}(t) - \theta_{1,1}(t)]}. \quad (59)$$

A similar equation can be obtained for the second delay cell

$$\frac{V2_1}{R} + jCV2_1 \frac{\mathrm{d}\theta_{2,1}(t)}{\mathrm{d}t} = \frac{2I_1}{\pi} e^{j[\theta_{1,1}(t) - \theta_{2,1}(t)]} + \frac{2I_2}{\pi}. \quad (60)$$

Appendix B
Stability Analysis of the Oscillation Phases of the Two-Stage Ring Oscillator

Equation (18) states that when the two-stage ring oscillator in Fig. 3 is free-running ($I_{\text{inj}} = 0$), the outputs have a phase difference of $\Delta\theta = \pm\pi/2$. In this section, we use perturbation analysis, a similar approach to that of [15], to investigate the stability of these solutions for $\Delta\theta$. We first start with $\Delta\theta = +\pi/2$. For this case, $\theta_{1,1}$ and $\theta_{2,1}$ can be expressed as

$$\theta_{1,1}(t) = \omega_{\text{SRF}} t + \delta\theta_1 \quad (61a)$$

$$\theta_{2,1}(t) = \omega_{\text{SRF}} t - \frac{\pi}{2} + \delta\theta_2 \quad (61b)$$

where $\delta\theta_1$ and $\delta\theta_2$ are perturbations added to $\theta_{1,1}$ and $\theta_{2,1}$, respectively. Substituting (61a) and (61b) into (15a) and (15b) results in

$$\omega_{\text{SRF}} + \frac{\mathrm{d}}{\mathrm{d}t}\delta\theta_1(t) = \frac{1}{RC} \frac{I_1 \cos\left(\delta\theta_1(t) - \delta\theta_2(t)\right)}{I_2 + I_1 \sin\left(\delta\theta_1(t) - \delta\theta_2(t)\right)} \quad (62a)$$

$$\omega_{\text{SRF}} + \frac{\mathrm{d}}{\mathrm{d}t}\delta\theta_2(t) = \frac{1}{RC} \frac{I_1 \cos\left(\delta\theta_1(t) - \delta\theta_2(t)\right)}{I_2 - I_1 \sin\left(\delta\theta_1(t) - \delta\theta_2(t)\right)}. \quad (62b)$$

If we define $\Delta(\delta\theta)$ as $\delta\theta_1 - \delta\theta_2$ and also considering that $\delta\theta_1$ and $\delta\theta_2$ are very small compared with $\theta_{1,1}$ and $\theta_{2,1}$, we can derive a differential equation for $\Delta(\delta\theta)$ using (62a) and (62b), as shown in the following:

$$\frac{\mathrm{d}}{\mathrm{d}t}\Delta\left(\delta\theta(t)\right) \approx -\frac{1}{\tau}\Delta\left(\delta\theta(t)\right) \quad (63)$$

where

$$\tau = \frac{1}{2\omega_{\text{SRF}}} \frac{I_2}{I_1}. \quad (64)$$

The solution to (63) is

$$\Delta\left(\delta\theta(t)\right) = \Delta\left(\delta\theta(0)\right) \exp(-t/\tau). \quad (65)$$

As can be seen from (65), any perturbation on the phase difference will eventually diminish. A similar analysis can be done for $\delta\theta_1(t)$ and $\delta\theta_2(t)$. From (62a), (62b), and (65), the solution for $\delta\theta_1(t)$ and $\delta\theta_2(t)$ can be expressed as follows:

$$\delta\theta_1(t) = \frac{I_2}{I_1} \frac{1}{2\tau} \left[\tau \ln\left(e^{t/\tau} + \frac{I_1}{I_2}\Delta\left(\delta\theta(0)\right)\right) - t\right] \quad (66a)$$

$$\delta\theta_2(t) = \frac{I_2}{I_1} \frac{1}{2\tau} \left[\tau \ln\left(e^{t/\tau} - \frac{I_1}{I_2}\Delta\left(\delta\theta(0)\right)\right) - t\right]. \quad (66b)$$

Using (66a) and (66b), it can be shown that $\lim_{t\to\infty} \delta\theta_1(t) = 0$ and $\lim_{t\to\infty} \delta\theta_2(t) = 0$.

A similar analysis for $\Delta\theta = -\pi/2$ results in

$$\Delta\left(\delta\theta(t)\right) = \Delta\left(\delta\theta(0)\right) \exp(+t/\tau) \quad (67)$$

which shows that, in this case, any perturbation sustains and grows with time. A similar analysis can be performed to check the stability of the solutions for oscillation phases in the presence of an external signal (I_{inj}).

References

[1] M. Farazian, "Fast hopping high-frequency carrier generation in digital CMOS technology," Ph.D. dissertation, Univ. California, San Diego, CA, May 2009.

[2] M. Farazian, P. Gudem, and L. Larson, "Fast hopping carrier generation for 14-band multi-band OFDM UWB in digital CMOS," in *Proc. Top. Meeting Silicon Monolithic Integr. Circuits RF Syst.*, Jan. 2010.

[3] C. Lin and C. Wang, "A regenerative semi-dynamic frequency divider for mode-1 MB-OFDM UWB hopping carrier generation," in *Proc. IEEE ISSCC Dig. Tech. Papers*, Feb. 2005, vol. 1, pp. 206–207.

[4] B. Razavi, *Phase-Locking in High-Performance Systems: From Devices to Architectures*. New York: Wiley, 2003.

[5] R. Miller, "Fractional-frequency generators utilizing regenerative modulation," *Proc. IRE*, vol. 27, no. 7, pp. 446–457, Jul. 1939.

[6] A. Safarian, S. Anand, and P. Heydari, "On the dynamics of regenerative frequency dividers," *IEEE Trans. Circuits Syst. II, Exp. Briefs*, vol. 53, no. 12, pp. 1413–1417, Dec. 2006.

[7] K. Sengupta, T. Bhattacharyya, and H. Hashemi, "A nonlinear transient analysis of regenerative frequency dividers," *IEEE Trans. Circuits Syst. I, Reg. Papers*, vol. 54, no. 12, pp. 2646–2660, Dec. 2007.

[8] H. Zheng and H. Luong, "A double-balanced quadrature-input quadrature-output regenerative frequency divider for UWB synthesizer applications," *IEEE Trans. Circuits Syst. I, Reg. Papers*, vol. 55, no. 9, pp. 2944–2951, Oct. 2008.
[9] J.-L. Li, S.-W. Qu, and Q. Xue, "A theoretical and experimental study of injection-locked fractional frequency dividers," *IEEE Trans. Microw. Theory Tech.*, vol. 56, no. 11, pp. 2399–2408, Nov. 2008.
[10] B. Razavi, "Heterodyne phase locking: A technique for high-frequency division," in *Proc. IEEE ISSCC Dig. Tech. Papers*, Feb. 2007, pp. 428–429.
[11] P. Larsson, "Fractional Frequency Divider," USA Patent 6 157 694, Dec. 5, 2000.
[12] B. Razavi, "A study of injection locking and pulling in oscillators," *IEEE J. Solid-State Circuits*, vol. 39, no. 9, pp. 1415–1424, Sep. 2004.
[13] M. Farazian, P. Gudem, and L. Larson, "A CMOS multi-phase injection-locked frequency divider for V-band operation," *IEEE Microw. Wireless Compon. Lett.*, vol. 19, no. 4, pp. 239–241, Apr. 2009.
[14] R. Adler, "A study of locking phenomena in oscillators," *Proc. IRE*, vol. 34, no. 6, pp. 351–357, Jun. 1946.
[15] A. Mirzaei, M. Heidari, R. Bagheri, and A. Abidi, "Multi-phase injection widens lock range of ring-oscillator-based frequency dividers," *IEEE J. Solid-State Circuits*, vol. 43, no. 3, pp. 656–671, Mar. 2008.
[16] J. Chien and L. Lu, "Analysis and design of wideband injection-locked ring oscillators with multiple-input injection," *IEEE J. Solid-State Circuits*, vol. 42, no. 9, pp. 1906–1915, Sep. 2007.
[17] G. Gangasani and P. Kinget, "Time-domain model for injection locking in nonharmonic oscillators," *IEEE Trans. Circuits Syst. I, Reg. Papers*, vol. 55, no. 6, pp. 1648–1658, Jul. 2008.
[18] S. Verma, H. Rategh, and T. Lee, "A unified model for injection-locked frequency dividers," *IEEE J. Solid-State Circuits*, vol. 38, no. 6, pp. 1015–1027, Jun. 2003.
[19] C. Mishra, A. Valdes-Garcia, F. Bahmani, A. Batra, E. Sanchez-Sinencio, and J. Silva-Martinez, "Frequency planning and synthesizer architectures for multiband OFDM UWB radios," *IEEE Trans. Microw. Theory Tech.*, vol. 53, no. 12, pp. 3744–3756, Dec. 2005.
[20] W. Yan and H. Luong, "A 900-MHz CMOS low-phase-noise voltage-controlled ring oscillator," *IEEE Trans. Circuits Syst. II, Analog Digit. Signal Process.*, vol. 48, no. 2, pp. 216–221, Feb. 2001.
[21] A. Hajimiri and T. Lee, "A general theory of phase noise in electrical oscillators," *IEEE J. Solid-State Circuits*, vol. 33, no. 2, pp. 179–194, Feb. 1998.
[22] A. Hajimiri, S. Limotyrakis, and T. Lee, "Phase noise in multi-gigahertz CMOS ring oscillators," in *Proc. IEEE Custom Integr. Circuits Conf.*, May 1998, pp. 49–52.
[23] Y. Kuo and R. Weng, "Regenerative frequency divider for 14 sub-band UWB applications," *Electron. Lett.*, vol. 44, no. 2, pp. 111–112, Jan. 2008.
[24] J. Rabaey, A. Chandrakasan, and B. Nikolic, *Digital Integrated Circuits*. Englewood Cliffs, NJ: Prentice-Hall, 2002.
[25] A. Ismail and A. Abidi, "A 3.1- to 8.2-GHz zero-IF receiver and direct frequency synthesizer in 0.18 μm SiGe BiCMOS for mode-2 MB-OFDM UWB communication," *IEEE J. Solid-State Circuits*, vol. 40, no. 12, pp. 2573–2582, Dec. 2005.
[26] Y. Wan, X. Lai, and J. Roychowdhury, "Understanding injection locking in negative-resistance LC oscillators intuitively using nonlinear feedback analysis," in *Proc. IEEE Custom Integr. Circuits Conf.*, Sep. 2005, pp. 729–732.

Mohammad Farazian (M'99) received the B.Sc. degree in electrical engineering from Sharif University of Technology, Tehran, Iran, in 2001, the M.Sc. degree in electrical engineering from the University of Tehran in 2003, and the Ph.D. degree in electrical engineering from the University of California San Diego, La Jolla, in 2009.

During the summer and fall of 2004, he was an Intern with Staccato Communications where he was working on the design of frequency synthesizers for UWB. From fall of 2007 to spring of 2008, he was an intern at Qualcomm Inc. and was working on the design of a SAW-less transmitter for cellular communications. He is now with Qualcomm Inc. where he is working on the design of frequency synthesizers for cellular communications. His research concentrates on the design of frequency synthesizers for wireless communications in digital CMOS technologies.

Dr. Farazian is the recipient of the 2009 Analog Devices Inc. Outstanding Student Designer Award and the second prize in the 2010 SiRF Student Paper Competition.

Prasad S. Gudem (M'96) received the B.Tech. degree in electrical engineering from the Indian Institute of Technology, Madras, India, in 1988 and the Ph.D. degree in electrical engineering from the University of Waterloo, Waterloo, ON, Canada, in 1996.

From 1997 to 2000, he was with Cadence Design Systems, San Diego, CA, where he was involved in semiconductor-device modeling for analog and RF applications. In 2000, he joined the IBM Watson Research Center, where he was involved with RF integrated-circuit design for WCDMA applications using IBM's SiGe technology. In 2002, he joined Qualcomm Inc., San Diego, as a Staff Engineer and led the development of diversity receivers for CDMA2000/WCDMA applications. As the Director of Engineering with the Analog/RF Integrated Circuit (IC) Design Group, Qualcomm Inc., he has continued to lead the development of next-generation transceivers for cellular applications. Since 2000, he has been teaching several graduate-level classes and coadvising several Ph.D. students in the area of RF IC design with the University of California San Diego, La Jolla.

Dr. Gudem was the recipient of the Graduate Teaching Award for the 2001–2002 academic year in recognition of his outstanding teaching of the ECE265 course sequence "Communication Circuit Design: I, II, and III."

Lawrence E. Larson (F'00) received the B.S. degree in electrical engineering from Cornell University, Ithaca, NY and the Ph.D. degree from the University of California, Los Angeles.

From 1980 to 1996, he was with Hughes Research Laboratories, Malibu, CA, where he directed the development of high-frequency microelectronics in GaAs, InP, Si/SiGe, and microelectromechanical systems (MEMS) technologies. He joined the faculty of the University of California San Diego (UCSD), La Jolla, in 1996, where he is the Inaugural Holder of the Communications Industry Chair. During the 2000–2001 academic year, he was on leave from IBM Research, San Diego. During the 2004 academic year, he was a Visiting Professor with Delft University of Technology, Delft, The Netherlands. From 2001 to 2006, he was the Director of the Center for Wireless Communications, UCSD. He is currently the Chair of the Department of Electrical and Computer Engineering, UCSD. He has published over 250 papers and has coauthored three books. He is the holder of 34 U.S. patents.

Dr. Larson was the recipient of the Hughes Sector Patent Award in 1994 for his work on RF MEMS, the corecipient of the 1996 Lawrence A. Hyland Patent Award of Hughes Electronics for his work on low-noise millimeterwave HEMTs, and the corecipient of the 1999 IBM Microelectronics Excellence Award for his work in Si/SiGe HBT technology.